Supporting Information for "Diffusion Selective Pulses"

Zhaoyuan Gong and Jamie D. Walls*

Department of Chemistry, University of Miami, Coral Gables, FL 33146

E-mail: jwalls@miami.edu

Phone: +001 305 284-4570. Fax: +001 305 284-4571

The following supporting information is provided: first, a few details about the calculations and superoperators introduced in the manuscript are provided. This is followed by a more in depth discussion about the mechanism behind the relaxation selective pulses used in this work. Plots of the diffusion selective pulses used in this work are also given, along with a table of spectral integrals in the 1:1:1:3 H_2O/DMSO/acetone/D_2O solution after application of diffusion selective pulses. Finally, details about the optimization algorithms used in generating relaxation/diffusion selective pulses are provided.

Additional details about theory in main paper

In Eq. (2) of the main paper, $\widehat{H}_{RF}(\omega_{RF}(t), \phi(t))$, which is the superoperator representing an RF pulse of amplitude $\omega_{RF}(t)$ and phase $\phi(t)$, is given by:

$$\widehat{H}_{RF}(\omega_{RF}, \phi) \;=\; i\omega_{RF} \begin{pmatrix} 0 & 0 & 0 & 0 \\ 0 & 0 & \frac{e^{-i\phi}}{2} & -\frac{e^{i\phi}}{2} \\ 0 & e^{i\phi} & 0 & 0 \\ 0 & -e^{-i\phi} & 0 & 0 \end{pmatrix} \tag{1}$$

The basic building block of implementing a diffusion selective pulse consists of placing an RF pulse in the middle of a GRE block, as shown in Fig. 2(A) in the main text. The reason for this is that the "zeroth"-order average Liouvillian for the k^{th} block for $k = 1$ to $k = N_c$, $\overline{\mathcal{L}^k}_{GRE}$ in Eq. (7) of the main text, is correct to second-order in terms of average Liouvillian theory[1] due to the symmetry of the evolution. Furthermore, keeping only the zeroth-order average Liouvillian in Eq. (7) of the main text and neglecting second-order and higher contributions is a reasonable approximation as long as $\theta_k = 2\pi\nu_{RF}t_k \ll \frac{\pi}{3}$. Furthermore, the condition $|\omega_I\tau_c| \ll \frac{\pi}{3}$ should also be observed in order to avoid any DANTE-like resonances[2] due to the inherent periodicity of the implementation of diffusion selective pulse given in Fig. 2(A) of the main text. In principle,

breaking this periodicity could be accomplished by varying the delays between GRE blocks, for example, although one would need to be careful that the same effective $T_2^{\text{Eff.}}$ was being generated in the different GRE blocks.

Mechanism behind relaxation selective pulses

As described in the main text, the majority of relaxation selective pulses consist of two basic steps: first, the initial equilibrium magnetization is attenuated and inverted by the relaxation selection pulse over a time $T_p - \tau_D$ from $\vec{M}_{eq}$ to $\vec{M}^{DSP}(T_2, T_1, T_p - \tau_D)$, which points along the $-\widehat{z}$-direction. The attenuation under the diffusion selective pulse, $\left|\vec{M}^{DSP}(T_2, T_1, T_p - \tau_D)\right|$, depends upon the T_1 and T_2 of spins and the details of the relaxation selective pulse. In the second step, the inverted magnetization undergoes a partial inversion recovery (T_1 relaxation) for a time $\tau_D = T_1^{\text{Sel}} \ln\left(\frac{M^{DSP}\left(T_2^{\text{Sel}}, T_1^{\text{Sel}}\right)}{M_{eq}} + 1\right)$, giving a total pulse length of T_p for the relaxation selective pulse. At the end of the relaxation selective pulse, those spins with $T_2 = T_2^{\text{Sel}}$ and $T_1 = T_1^{\text{Sel}}$ have had their magnetization nulled, i.e., $\left|M^{DSP}(T_2^{\text{Sel}}, T_1^{\text{Sel}}, T_p)\right| \approx 0$. Typically for spins with $T_2 < T_2^{\text{Sel}}$, $\left|\vec{M}^{DSP}(T_2, T_1, T_p - \tau_D)\right| < \left|\vec{M}^{DSP}(T_2^{\text{Sel}}, T_1^{\text{Sel}}, T_p - \tau_D)\right|$ and thus $\vec{M}^{DSP}(T_2, T_1, T_p)$ ends up with $\widehat{z}$-magnetization oriented along the $+\widehat{z}$-direction after the inversion recovery period. For species with $T_2 > T_2^{\text{Sel}}$,

$\left|\vec{M}^{DSP}(T_2, T_1, T_p - \tau_D)\right| > \left|\vec{M}^{DSP}(T_2^{\text{Sel}}, T_1^{\text{Sel}}, T_p - \tau_D)\right|$ and thus $\vec{M}^{DSP}(T_2, T_1, T_p)$ ends up with $\widehat{z}$-magnetization still oriented along the $-\widehat{z}$-direction after the inversion recovery period. This behavior is illustrated in Fig. 1 which shows the trajectories for magnetization under diffusion selective pulses used in Fig. 2 and Fig. 4(C) of the main paper (the latter pulse is given in Fig. 3(A) in Supporting Information). As discussed above, the magnetization is inverted in all cases and then undergoes T_1 relaxation whereby those species with $T_2 = T_2^{\text{Sel}}$ are suppressed.

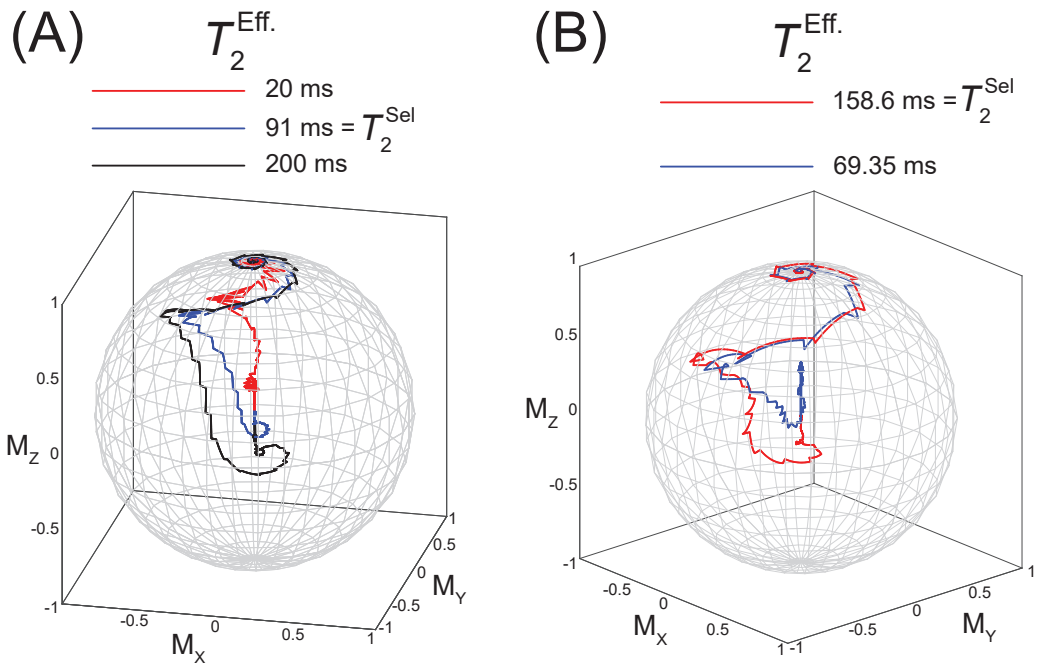

Figure 1: Trajectories of the magnetization vectors with different values of T_2 under two different diffusion selective pulses. (A) Under the diffusion selective pulse designed to suppress the magnetization for species with $T_2^{\text{Sel}} = 91$ ms ($T_p = 1.8408$ s) used in Fig. 2 in the main manuscript, the trajectories of the magnetization for species with $T_2 = 20$ ms (red curve), $T_2 = 91$ ms = T_2^{Sel} (blue curve), and $T_2 = 200$ ms (black curve) are shown. In all case, the magnetization is inverted from equilibrium, after which the magnetization undergoes inversion recovery. For $T_2 = 20$ ms $< T_2^{\text{Sel}}$ (red curve), the magnetization ends up being oriented along the $+\widehat{z}$-direction; for $T_2 = 200$ ms $> T_2^{\text{Sel}}$ (black curve), the magnetization ends up being along $-\widehat{z}$-direction, and for $T_2 = T_2^{\text{Sel}} = 91$ ms (blue curve), the magnetization ends up being nulled at time $T_p = 1.8408$ s. (B) The trajectories of the magnetization during the diffusion selective pulse used in Fig. 4(C) in the main paper [and given in Fig. 3(A)] are shown for species with $T_2 = 69.35$ ms (blue curve) and $T_2 = T_2^{\text{Sel}} = 158.6$ ms (red curve). Similar to the trajectories in (A), the diffusion selective pulse ends up inverting the magnetization of both species although the species with $T_2 = 69.35$ ms $< T_2^{\text{Sel}}$ ends up with magnetization along the $+\widehat{z}$-direction (blue curve) whereas the species with $T_2 = T_2^{\text{Sel}} = 158.6$ ms ends up being nulled at the end of the diffusion selective pulse.

Diffusion selective pulses used in Figs. 3 and 4 of the main text

Figures 2 and 3 give the pulse lengths, t_k, and phases ϕ_k, for the diffusion selective pulses used in Fig. 3 and Fig. 4 in the main text. In Fig. 2, the diffusion selective pulses were implemented using the sequence in Fig. 2(A) in order to selectively suppress signals in a 1:1:1:3 v/v/v/v H_2O/DMSO/acetone/D_2O solution based upon the effective relaxation times under the GRE blocks. The water, acetone, and DMSO resonances were suppressed using the diffusion selective pulses given in Fig. 2(B), 2(C), and 2(D), respectively.

The integrals of the spectra in the H_2O/DMSO/acetone solution [Fig. 3(C) in the main text] from the remaining transverse and $\widehat{z}-$ magnetization after application of diffusion selective pulses given in Fig. 2 are given in Table 1. In most cases, the resulting attenuation of magnetization after application of the diffusion selective pulses was typically less than the theoretical predictions given by Eq. (6) in the main text, although in some cases larger signals were observed as given in Table 1. In these cases, differences in $T_{1,I}$ and/or chemical shifts can reduce the overall magnetization attenuation of the diffusion selective pulses as predicted from Eq. (6) in the main text. In Fig. 3, diffusion selective pulses that were used in the imaging experiments shown in Figure 4 of the main text are present with additional details given in Fig. 3's caption.

Application of the GRAPE method to optimize RF pulses

In many problems in NMR, we are interested in finding an RF pulse, $\left(\omega^{RF}(t)\right)_{\phi(t)}$, that minimizes a given cost functional, $\Phi\left[\Omega_{\text{spectral}}, (\omega^{RF}(t))_{\phi(t)}, \eta_{RF}, \omega_Z, \vec{M}(T_p)\right]$, which depends upon the spectral parameters [$\Omega_{\text{spectral}} \in T_1$, T_2, chemical shifts, J-couplings, etc.], RF and B_0 inhomogeneity, which are represented by η_{RF} and ω_Z, respectively [where the dimensionless parameter η_{RF} represents an RF scaling factor with $\eta_{RF} = 1$ for a perfectly calibrated pulse, and ω_Z represents a local resonance offset], and the final state of the magnetization at the end of the RF pulse of length T_p,

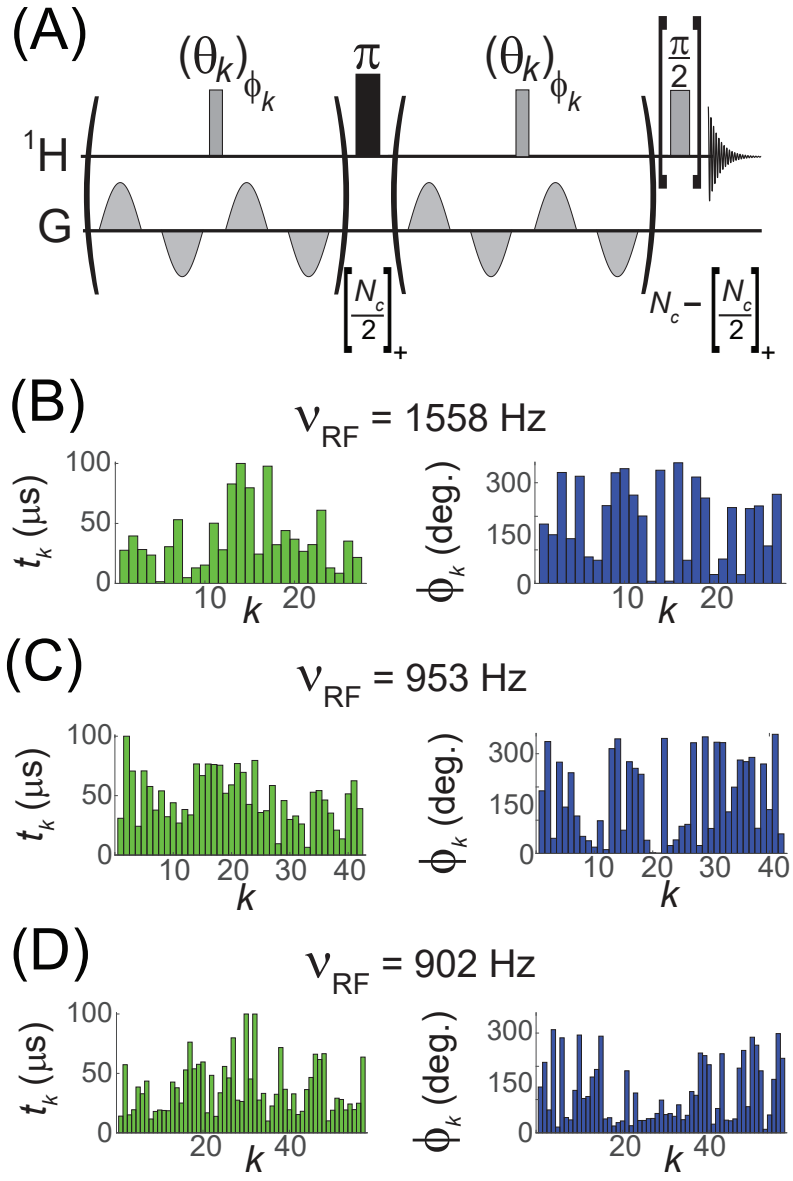

Figure 2: Diffusion selective pulses designed to selectively suppress signals in a 1:1:1:3 H_2O/DMSO/acetone/D_2O solution used in Fig. 3 of the main text. (A) The basic pulse sequence used to implement the diffusion selective pulses, where a π-pulse was placed roughly in the middle ($[z]_+$ = ceiling of z) of the sequence. In all experiments, $g = 44.7$ G/cm, $\delta = 3$ ms, $\Delta = 4$ ms, $t_d = 400\,\mu$s, $\tau_c = 15.6$ ms, and the RF transmitter was placed at the average frequency offset of $\delta_{\text{transmitter}} = 3.22$ ppm. (B) Diffusion selective pulse ($N_c = 27$, $\nu_{RF} = 1558$ Hz, $T_p = 421.2$ ms, and $T_2^{\text{Sel}} = 37$ ms) designed to suppress the water resonance. (C) Diffusion selective pulse ($N_c = 42$, $\nu_{RF} = 953$ Hz, $T_p = 655.2$ ms, and $T_2^{\text{Sel}} = 58$ ms) designed to suppress the acetone resonance. (D) Diffusion selective pulse ($N_c = 57$, $\nu_{RF} = 902$ Hz, $T_p = 889.2$ ms, and $T_2^{\text{Sel}} = 71$ ms) designed to suppress the DMSO resonance. The spectra after application of the diffusion selective pulses were given in Fig. 3(C) of the main text with the corresponding integrals of the spectra given in Table 1.

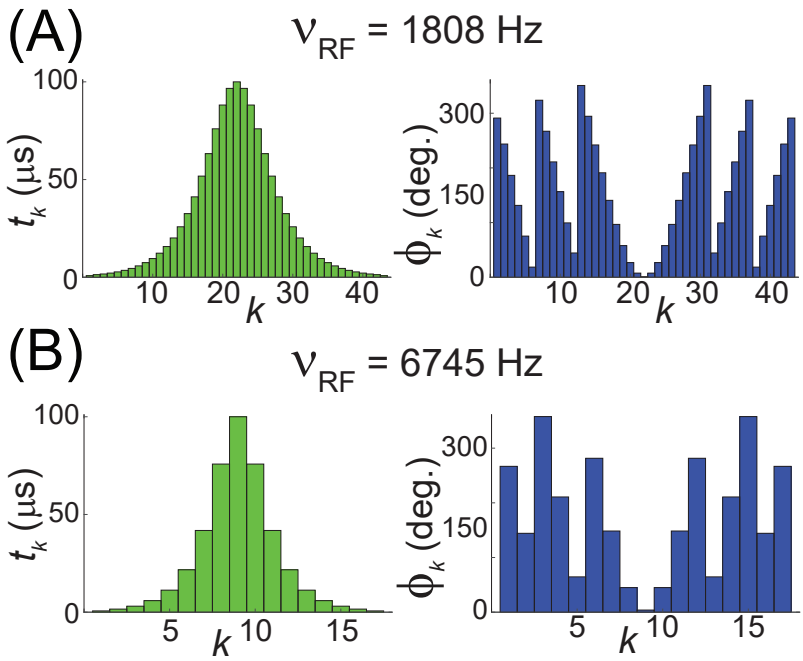

Figure 3: Diffusion selective pulses designed to selectively suppress signals in an imaging phantom used in Figure 4 of the main text. In all experiments, $g = 23.92$ G/cm, $\delta = 3$ ms, $\Delta = 5.11$ ms, $t_d = 500\,\mu$s, and $\tau_c = 18.45$ ms. (B) Diffusion selective pulse ($N_c = 43$, $\nu_{RF} = 1808$ Hz, $T_p = 793.35$ ms, and $T_2^{\text{Sel}} = 158.6$ ms) designed to suppress the water resonance in a 1:1 v/v H_2O/DMSO-d_6 solution with pH$= 4.56$ (placed in 2mm coaxial insert). (C) Diffusion selective pulse ($N_c = 17$, $\nu_{RF} = 6745$ Hz, $T_p = 313.65$ ms, and $T_2^{\text{Sel}} = 69.35$ ms) designed to suppress the water resonance in a [Gd^{+3}]=88μM solution in 1:1 v/v H_2O/D_2O sample (placed in outer 5mm tube). Images taken after application of these diffusion selective pulses were given in Fig. 4(C) and 4(D) of the main text.

Table 1: Observed integrals for diffusion-selective pulses [Fig. 2] applied to a 1:1:1:3 v/v/v/v DMSO/acetone/H_2O/D_2O solution [Fig. 3 from main text]

T_2^{sel} (ms)	Species	$\left\lvert\frac{M_Z}{M_{eq}}\right\rvert$	$\left\lvert\frac{M_+}{M_{eq}}\right\rvert$	$\left\lvert\frac{\vec{M}}{M_{eq}}\right\rvert_{\text{Theor.}}$ [Eq. 6 (main text)]
[Fig. 2(B)] 37.1	DMSO	3.33×10^{-1}	7.7×10^{-2}	3.14×10^{-1}
	acetone	1.23×10^{-1}	1.9×10^{-3}	2.22×10^{-1}
	H_2O	1.3×10^{-2}	2×10^{-3}	0
[Fig. 2(C)] 58.3	DMSO	7.0×10^{-2}	3×10^{-3}	9.9×10^{-2}
	acetone	6×10^{-3}	3×10^{-3}	0
	H_2O	2.5×10^{-2}	1.3×10^{-2}	2.22×10^{-1}
[Fig. 2(D)] 71.2	DMSO	6×10^{-3}	3×10^{-3}	0
	acetone	1.24×10^{-1}	2.1×10^{-2}	9.9×10^{-2}
	H_2O	2.54×10^{-1}	8.8×10^{-2}	3.14×10^{-1}

$\vec{M}(T_p) = M_Z(T_p)\widehat{z} + M_X(T_p)\widehat{x} + M_Y(T_p)\widehat{y}$, which can be calculated from:

$$\begin{aligned}
\mathbf{M}(T_p) &= \begin{pmatrix} 1 \\ M_Z(T_p) \\ M_X(T_p) \\ M_Y(T_p) \end{pmatrix} = 1 + \vec{M}(T_p) \\
&= \widehat{T}\exp\left(\int_0^{T_p} \mathrm{d}t' \left[\eta_{RF}\left(\omega_X^{RF}(t')\widehat{\widehat{I}}_X + \omega_Y^{RF}(t')\widehat{\widehat{I}}_Y\right) + \omega_Z\widehat{\widehat{I}}_Z + \widehat{\widehat{\mathcal{L}}}(\Omega_{\text{spectral}})\right]\right)\mathbf{M}(0) \qquad (2) \\
\vec{M}(T_p) &= \left(\widehat{z}\,(\widehat{z})^{\mathrm{T}} + \widehat{x}\,(\widehat{x})^{\mathrm{T}} + \widehat{y}\,(\widehat{y})^{\mathrm{T}}\right)\widehat{\mathbf{M}}(T_p) \qquad (3)
\end{aligned}$$

where $\widehat{T}$ represents the Dyson-time ordering operator, $\widehat{z} = \begin{pmatrix} 0 \\ 1 \\ 0 \\ 0 \end{pmatrix}$, $\widehat{x} = \begin{pmatrix} 0 \\ 0 \\ 1 \\ 0 \end{pmatrix}$, $\widehat{y} = \begin{pmatrix} 0 \\ 0 \\ 0 \\ 1 \end{pmatrix}$, and $\mathbf{M}(0) = 1 + \vec{M}(0) = 1 + M_{eq}\widehat{z}$. In Eq. (2), $\widehat{\widehat{I}}_X$, $\widehat{\widehat{I}}_Y$ and $\widehat{\widehat{I}}_Z$ represent spin-1/2 superoperators,

which are given by:

$$\begin{aligned}
\widehat{\widehat{I}}_Z &= \begin{pmatrix} 0 & 0 & 0 & 0 \\ 0 & 0 & 0 & 0 \\ 0 & 0 & 0 & 1 \\ 0 & 0 & -1 & 0 \end{pmatrix} \\
\widehat{\widehat{I}}_X &= \begin{pmatrix} 0 & 0 & 0 & 0 \\ 0 & 0 & 0 & -1 \\ 0 & 0 & 0 & 0 \\ 0 & 1 & 0 & 0 \end{pmatrix} \\
\widehat{\widehat{I}}_Y &= \begin{pmatrix} 0 & 0 & 0 & 0 \\ 0 & 0 & 1 & 0 \\ 0 & -1 & 0 & 0 \\ 0 & 0 & 0 & 0 \end{pmatrix}
\end{aligned} \tag{4}$$

and $\widehat{\widehat{\mathcal{L}}}(\Omega_{\text{spectral}})$ represents the time-independent Liouvillian during the time T_p. When $\left(\omega^{RF}(t)\right)_{\phi(t)}$ can be approximated by a series of N, piecewise constant rectangular pulses as illustrated in Fig. 4, where the amplitude, phase, and length of the $k^{th}-$ pulse is given by ω_k^{RF}, ϕ_k, and τ_k, respectively, then $\mathbf{M}(T_p)$ with $T_p = \sum_{k=1}^{N} \tau_k$ can be approximated by:

$$\begin{aligned}
\mathbf{M}(T_p) &\approx \left(\widehat{T} \prod_{k=1}^{N} \widehat{V}_k(\Omega_{\text{spectral}}, \omega_Z, \eta_{RF}, \omega_{X,k}^{RF}, \omega_{Y,k}^{RF}, \tau_k) \right) \mathbf{M}(0) \\
&\approx 1 + \vec{M}(T_p) = 1 + \left(\widehat{z}\,(\widehat{z})^{\mathsf{T}} + \widehat{x}\,(\widehat{x})^{\mathsf{T}} + \widehat{y}\,(\widehat{y})^{\mathsf{T}} \right) \widehat{\mathbf{M}}(T_p)
\end{aligned} \tag{5}$$

where $\omega_{X,k}^{RF} = \omega_k^{RF} \cos(\phi_k)$, $\omega_{Y,k}^{RF} = \omega_k^{RF} \sin(\phi_k)$, and

$$\widehat{V}_k(\Omega_{\text{spectral}}, \omega_Z, \eta_{RF}, \omega_{X,k}^{RF}, \omega_{Y,k}^{RF}, \tau_k) = \exp\left(\tau_k \left[\eta_{RF} \left(\omega_{X,k}^{RF} \widehat{\widehat{I}}_X + \omega_{Y,k}^{RF} \widehat{\widehat{I}}_Y \right) + \omega_Z \widehat{\widehat{I}}_Z + \widehat{\widehat{\mathcal{L}}}(\Omega_{\text{spectral}}) \right] \right) \tag{6}$$

represents the propagator during the time $\sum_{j=1}^{k-1}\tau_j \leq t \leq \sum_{j=1}^{k}\tau_j$ under the k^{th} rectangular pulse.

For a T_2- selective pulse, the cost functional $\Phi\left[\Omega_{\text{spectral}}, \eta_{RF}, \omega_Z, \vec{M}(T_p)\right]$ should be minimized for a $\left(\omega^{RF}(t)\right)_{\phi(t)}$ that results in $\left|\vec{M}(T_p)\right| \approx 0$ for $T_2 = T_2^{\text{Sel}}$ while minimally attenuating $|\vec{M}(T_p)|$ for those spins with $T_2 \neq T_2^{\text{Sel}}$. One way to find such an $\left(\omega^{RF}(t)\right)_{\phi(t)}$ is by using the GRAPE algorithm.[3] The GRAPE algorithm works as follows: defining the following propagators for $k = 1$ to $k = N$:

$$\widehat{\widehat{U}}_k^F = \widehat{T}\prod_{j=1}^{k}\widehat{\widehat{V}}_j(\Omega_{\text{spectral}}, \omega_Z, \eta_{RF}, \omega_{X,j}^{RF}, \omega_{Y,j}^{RF}, \tau_j) \tag{7}$$

along with $\widehat{\widehat{U}}_1^B = \widehat{\widehat{1}}$, and

$$\widehat{\widehat{U}}_k^B = \widehat{T}\prod_{j=2}^{k}\widehat{\widehat{V}}_{N-j+2}(\Omega_{\text{spectral}}, \omega_Z, \eta_{RF}, \omega_{X,N-j+2}^{RF}, \omega_{Y,N-j+2}^{RF}, \tau_{N-j+2}) \tag{8}$$

for $k = 2$ to $k = N$, $\vec{M}(T_p)$ can be determined from Eq. (5) by:

$$\vec{M}(T_p) \;=\; \left(\widehat{z}\,(\widehat{z})^{\text{T}} + \widehat{x}\,(\widehat{x})^{\text{T}} + \widehat{y}\,(\widehat{y})^{\text{T}}\right)\widehat{\widehat{U}}_N^F\widehat{\mathbf{M}}(0) \tag{9}$$

where we used the fact that $\mathbf{M}(T_p) = \widehat{\widehat{U}}_N^F\mathbf{M}(0)$. Denoting $\vec{\omega}_X^{RF} = \left(\omega_{X,1}^{RF},\, \omega_{X,2}^{RF},\, \cdots, \omega_{X,N-1}^{RF},\, \omega_{X,N}^{RF}\right)$ and $\vec{\omega}_Y^{RF} = \left(\omega_{Y,1}^{RF},\, \omega_{Y,2}^{RF},\, \cdots, \omega_{Y,N-1}^{RF},\, \omega_{Y,N}^{RF}\right)$, the GRAPE algorithm finds the appropriate $\vec{\omega}_X^{RF}$ and $\vec{\omega}_Y^{RF}$ that minimize Φ by updating the k^{th} pulse to $\left(\omega_{X,k}^{RF}\right)^{\text{new}} = \left(\omega_{X,k}^{RF}\right)^{\text{old}} - \lambda_{\text{step}}\overline{\delta\omega}_{X,k}$ and $\left(\omega_{Y,k}^{RF}\right)^{\text{new}} = \left(\omega_{Y,k}^{RF}\right)^{\text{old}} - \lambda_{\text{step}}\overline{\delta\omega}_{Y,k}$ for $k = 1$ to $k = N$, where:

$$\begin{aligned}
\overline{\delta\omega}_{X,k} &= \left\langle\left(\frac{\delta\Phi}{\delta M_Z}\overline{z}^{\text{T}} + \frac{\delta\Phi}{\delta M_X}\overline{x}^{\text{T}} + \frac{\delta\Phi}{\delta M_Y}\overline{y}^{\text{T}}\right)\left(\eta_{RF}\tau_k\widehat{\widehat{U}}_{N-k+1}^B\widehat{\widehat{H}}_X\widehat{\widehat{U}}_k^F\widehat{\mathbf{M}}(0)\right)\right\rangle \\
\overline{\delta\omega}_{Y,k} &= \left\langle\left(\frac{\delta\Phi}{\delta M_Z}\overline{z}^{\text{T}} + \frac{\delta\Phi}{\delta M_X}\overline{x}^{\text{T}} + \frac{\delta\Phi}{\delta M_Y}\overline{y}^{\text{T}}\right)\left(\eta_{RF}\tau_k\widehat{\widehat{U}}_{N-k+1}^B\widehat{\widehat{H}}_Y\widehat{\widehat{U}}_k^F\widehat{\mathbf{M}}(0)\right)\right\rangle
\end{aligned} \tag{10}$$

In Eq. (10), $\langle\cdots\rangle$ represents a (possible) average over parameters [e.g., T_2's, η_{RF}, ω_Z, etc.], and

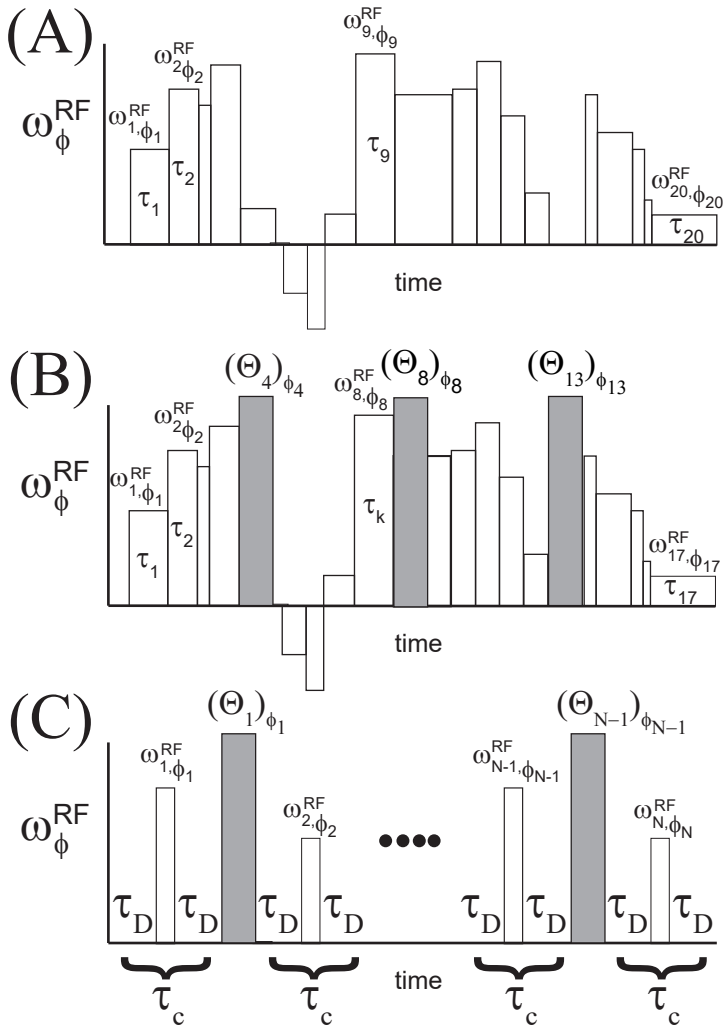

Figure 4: (A) An RF pulse, $\left(\omega^{RF}(t)\right)_{\phi(t)}$, that is approximated by N, piecewise constant rectangular pulses, where the k^{th} pulse has amplitude, phase, and length of ω_k^{RF}, ϕ_k, and τ_k, respectively. As illustrated in (A), the $\left(\omega^{RF}(t)\right)_{\phi(t)}$ was approximated by $N = 20$ rectangular pulses. In the GRAPE algorithm,[3] the individual ω_k^{RF} and ϕ_k are optimized by iterating Eq. (10). (B) The GRAPE algorithm can also be used to optimize the individual ω_k^{RF} and ϕ_k in the presence of fixed RF pulses [$(\Theta_4)_{\phi_4}-$, $(\Theta_8)_{\phi_8}-$, and $(\Theta_{13})_{\phi_{13}}-$ pulses as illustrated in (B)] by iterating Eq. (15). (C) For a pulse sequence consisting of N small-flip $(\theta_k)_{\phi_k}-$ pulses with $\theta_k = \omega_k^{RF} t_p$ applied in between periods of free evolution of time τ_D (with $\tau_c = 2\tau_D + t_p$) and fixed RF pulses, the individual ω_k^{RF} and ϕ_k of the $(\theta_k)_{\phi_k}-$ pulses can be optimized by iterating Eq. (19).

$\frac{\delta\Phi}{\delta M_j}$ represents functional derivatives of Φ with respect to M_j for $j = X, Y, Z$. In this case, the algorithm is iterated until convergence is achieved (additional details of the implementation, such as line searches to determine the best λ_{step} and time scaling, have been previously reported[4]).

Optimizing $\left(\omega^{RF}(t)\right)_{\phi(t)}$ in the presence of a fixed set of RF pulses

In some instances, $\left(\omega^{RF}(t)\right)_{\phi(t)}$ needs to be applied in the presence of a series of fixed, RF pulses, e.g., applying a selective excitation pulse in the presence of homonuclear decoupling[5] or requiring a $\pi-$ pulse be applied in the middle of the sequence to refocus B_0 inhomogeneity, etc. In this case, a modified version of the GRAPE algorithm can be employed. Consider determining a $\left(\omega^{RF}(t)\right)_{\phi(t)}$ that minimizes some cost function Φ in the presence of a set of fixed RF pulses. Assume again that $\left(\omega^{RF}(t)\right)_{\phi(t)}$ can be represented by N, piecewise constant rectangular pulses, but with up to N additional, fixed RF pulses that are interspersed within the sequence. This is illustrated in Fig. 4(B), where $N = 17$, and three different, fixed RF pulses are applied: a $(\Theta_4)_{\phi_4}-$ pulse [applied directly after the $\left(\omega_4^{RF}\right)_{\phi_4} -$ pulse], a $(\Theta_8)_{\phi_8}-$ pulse [applied directly after the $\left(\omega_8^{RF}\right)_{\phi_8} -$ pulse], and a $(\Theta_{13})_{\phi_{13}}-$ pulse [applied directly after the $\left(\omega_{13}^{RF}\right)_{\phi_{13}} -$ pulse]. Defining the following propagators for $k = 1$ to $k = N$:

$$\widehat{\widehat{U}}^{F}_{RF,k} \;=\; \widehat{T}\prod_{j=1}^{k}\widehat{\widehat{R}}_j\widehat{\widehat{V}}_j(\Omega_{\text{spectral}}, \omega_Z, \eta_{RF}, \omega^{RF}_{X,j}, \omega^{RF}_{Y,j}, \tau_j) \tag{11}$$

where $\widehat{\widehat{V}}_j$ is given in Eq. (6), and

$$\widehat{\widehat{R}}_j \;=\; \exp\left(t_j\left[\eta_{RF}\left(\frac{\Theta_j}{t_j}\cos(\phi_j)\widehat{\widehat{I}}_X + \frac{\Theta_j}{t_j}\sin(\phi_j)\widehat{\widehat{I}}_Y\right) + \omega_Z\widehat{\widehat{I}}_Z + \widehat{\widehat{\mathcal{L}}}(\Omega'_{\text{Spectral}})\right]\right) \tag{12}$$

represents the propagator for a rectangular RF pulse pulse of length t_j with a nominal flip angle of $\Theta_j \neq 0$. If $\Theta_j = 0$, then $t_j = 0$ and so $\widehat{\widehat{R}}_j = \widehat{\widehat{1}}$ representing the fact that no RF pulse was applied.

Note that in Eq. (12), $\widehat{\widehat{\mathcal{L}}}(\Omega'_{\text{Spectral}})$ need not be the same as $\widehat{\widehat{\mathcal{L}}}(\Omega_{\text{spectral}})$ found in Eq. (6).

Further define $\widehat{\widehat{U}}^{B}_{RF,1} = \widehat{\widehat{1}}$, and

$$\widehat{\widehat{U}}^{B}_{k} = \widehat{T}\prod_{j=2}^{k}\widehat{\widehat{R}}_{N-j+2}\widehat{\widehat{V}}_{N-j+2}(\Omega_{\text{spectral}},\omega_Z,\eta_{RF},\omega^{RF}_{X,N-j+2},\omega^{RF}_{Y,N-j+2},\tau_{N-j+2}) \tag{13}$$

for $k = 2$ to $k = N$, $\vec{M}(T_p)$ can be written as:

$$\vec{M}(T_p) \;=\; \left(\widehat{z}\,(\widehat{z})^{\mathrm{T}} + \widehat{x}\,(\widehat{x})^{\mathrm{T}} + \widehat{y}\,(\widehat{y})^{\mathrm{T}}\right)\widehat{\widehat{U}}^{F}_{RF,N}\widehat{\mathbf{M}}(0) \tag{14}$$

In this case, the GRAPE algorithm can be used to find the appropriate $\vec{\omega}^{RF}_X$ and $\vec{\omega}^{RF}_Y$ that minimize Φ by updating the k^{th} pulse to $\left(\omega^{RF}_{X,k}\right)^{\text{new}} = \left(\omega^{RF}_{X,k}\right)^{\text{old}} - \lambda_{\text{step}}\overline{\delta\omega}_{X,k}$ and $\left(\omega^{RF}_{Y,k}\right)^{\text{new}} = \left(\omega^{RF}_{Y,k}\right)^{\text{old}} - \lambda_{\text{step}}\overline{\delta\omega}_{Y,k}$ for $k = 1$ to $k = N$, where

$$\begin{aligned}
\overline{\delta\omega}_{X,k} &= \left\langle\left(\frac{\delta\Phi}{\delta M_Z}\overline{z}^{\mathrm{T}} + \frac{\delta\Phi}{\delta M_X}\overline{x}^{\mathrm{T}} + \frac{\delta\Phi}{\delta M_Y}\overline{y}^{\mathrm{T}}\right)\left(\eta_{RF}\tau_k\widehat{\widehat{U}}^{B}_{RF,N-k+1}\widehat{\widehat{R}}_k\widehat{\widehat{H}}_X\left(\widehat{\widehat{R}}_k\right)^{-1}\widehat{\widehat{U}}^{F}_{RF,k}\widehat{\mathbf{M}}(0)\right)\right\rangle \\
\overline{\delta\omega}_{Y,k} &= \left\langle\left(\frac{\delta\Phi}{\delta M_Z}\overline{z}^{\mathrm{T}} + \frac{\delta\Phi}{\delta M_X}\overline{x}^{\mathrm{T}} + \frac{\delta\Phi}{\delta M_Y}\overline{y}^{\mathrm{T}}\right)\left(\eta_{RF}\tau_k\widehat{\widehat{U}}^{B}_{RF,N-k+1}\widehat{\widehat{R}}_k\widehat{\widehat{H}}_Y\left(\widehat{\widehat{R}}_k\right)^{-1}\widehat{\widehat{U}}^{F}_{RF,k}\widehat{\mathbf{M}}(0)\right)\right\rangle
\end{aligned} \tag{15}$$

Eq. (15) can be iterated until a desired level of convergence has been achieved.

Optimizing a series of small flip-angle pulses

When implementing diffusion selective pulses, pulsed field gradient blocks were utilized to generate an effective Liouvillian over the time τ_c, with $(\theta_k)_{\phi_k}$ – pulses of fixed length t_p placed in the middle of the pulsed field gradient blocks in order to generate a diffusion selective pulse, where $\theta_k = \omega^{RF}_k t_p$. This is illustrated in Fig. 4(C). In this case, for a given $\widehat{\widehat{L}}(\Omega''_{\text{spectral}})$ that was generated during the times τ_C, the various small-flip pulses can be optimized in order to minimize a given Φ.

Let $\widehat{\widehat{U}}_D = \exp\left(\tau_D \widehat{\widehat{L}}(\Omega''_{\text{spectral}})\right)$, and define the following propagators for $k = 1$ to $k = N$:

$$\widehat{\widehat{U}}^F_{\text{delay},k} = \widehat{T}\prod_{j=1}^{k}\widehat{\widehat{R}}_j\widehat{\widehat{U}}_D\widehat{\widehat{V}}_j(\Omega_{\text{spectral}},\omega_Z,\eta_{RF},\omega^{RF}_{X,j},\omega^{RF}_{Y,j},t_p)\widehat{\widehat{U}}_D \tag{16}$$

where $\widehat{\widehat{V}}_j$ is given in Eq. (6), and $\widehat{\widehat{R}}_j$ is defined in Eq. (12). Note that $\widehat{\widehat{L}}(\Omega_{\text{spectral}})$ during the small-flip angle pulses may be different than the $\widehat{\widehat{L}}(\Omega''_{\text{spectral}})$ during the times τ_D and $\widehat{\widehat{L}}(\Omega'_{\text{spectral}})$ during the fixed RF pulses. Further, define $\widehat{\widehat{U}}^B_{\text{delay},1} = \widehat{\widehat{1}}$, and

$$\widehat{\widehat{U}}^B_{\text{delay},k} = \widehat{T}\prod_{j=2}^{k}\widehat{\widehat{R}}_{N-j+2}\widehat{\widehat{U}}_D\widehat{\widehat{V}}_{N-j+2}(\Omega_{\text{spectral}},\omega_Z,\eta_{RF},\omega^{RF}_{X,N-j+2},\omega^{RF}_{Y,N-j+2},t_p)\widehat{\widehat{U}}_D \tag{17}$$

for $k = 2$ to $k = N$, then $\vec{M}(T_p)$ can be written as:

$$\vec{M}(T_p) = \left(\widehat{z}\,(\widehat{z})^{\text{T}} + \widehat{x}\,(\widehat{x})^{\text{T}} + \widehat{y}\,(\widehat{y})^{\text{T}}\right)\widehat{\widehat{U}}^F_{\text{delay},N}\widehat{\mathbf{M}}(0) \tag{18}$$

In this case, the GRAPE algorithm finds the appropriate $\vec{\omega}^{RF}_X$ and $\vec{\omega}^{RF}_Y$ for the small-flip angle pulses that minimize Φ by updating the k^{th} pulse to $\left(\omega^{RF}_{X,k}\right)^{\text{new}} = \left(\omega^{RF}_{X,k}\right)^{\text{old}} - \lambda_{\text{step}}\overline{\delta\omega}_{X,k}$ and $\left(\omega^{RF}_{Y,k}\right)^{\text{new}} = \left(\omega^{RF}_{Y,k}\right)^{\text{old}} - \lambda_{\text{step}}\overline{\delta\omega}_{Y,k}$ for $k = 1$ to $k = N$, where

$$\begin{aligned}
\overline{\delta\omega}_{X,k} &= \left\langle\left(\frac{\delta\Phi}{\delta M_Z}\overline{z}^{\text{T}} + \frac{\delta\Phi}{\delta M_X}\overline{x}^{\text{T}} + \frac{\delta\Phi}{\delta M_Y}\overline{y}^{\text{T}}\right)\left(\eta_{RF}t_p\widehat{\widehat{U}}^B_{\text{delay},N-k+1}\widehat{\widehat{R}}_k\widehat{\widehat{U}}_D\widehat{\widehat{H}}_X\left(\widehat{\widehat{U}}_D\right)^{-1}\left(\widehat{\widehat{R}}_k\right)^{-1}\widehat{\widehat{U}}^F_{\text{delay},k}\widehat{\mathbf{M}}(0)\right)\right\rangle \\
\overline{\delta\omega}_{Y,k} &= \left\langle\left(\frac{\delta\Phi}{\delta M_Z}\overline{z}^{\text{T}} + \frac{\delta\Phi}{\delta M_X}\overline{x}^{\text{T}} + \frac{\delta\Phi}{\delta M_Y}\overline{y}^{\text{T}}\right)\left(\eta_{RF}t_p\widehat{\widehat{U}}^B_{\text{delay},N-k+1}\widehat{\widehat{R}}_k\widehat{\widehat{U}}_D\widehat{\widehat{H}}_Y\left(\widehat{\widehat{U}}_D\right)^{-1}\left(\widehat{\widehat{R}}_k\right)^{-1}\widehat{\widehat{U}}^F_{\text{delay},k}\widehat{\mathbf{M}}(0)\right)\right\rangle
\end{aligned} \tag{19}$$

Eq. (19) can be iterated until some desired level of convergence has been achieved. The diffusion selective pulses in Fig. 4 of the manuscript utilized this version of the GRAPE algorithm.

Acknowledgments

We would like to acknowledge support from the National Science Foundation under CHE - 1626015 and CHE - 1807724.

References

(1) Levitt, M. H.; Dibari, L. Steady-State in Magnetic Resonance Pulse Experiments. *Phys. Rev. Lett.* **1992**, *69*, 3124–3127.

(2) Walls, J. D.; Coomes, A. Pseudorandom Selective Excitation in NMR. *J. Mag. Res.* **2011**, *212*, 186–196.

(3) Khaneja, N.; Reiss, T.; Kehlet, C.; Schulte-Herbruggen, T.; Glaser, S. J. Optimal Control of Coupled Spin Dynamics: Design of NMR Pulse Sequences by Gradient Ascent Algorithms. *Journal of Magnetic Resonance* **2005**, *172*, 296–305.

(4) Lopez, C. J.; Lu, W.; Walls, J. D. Relaxation Selective Pulses in Fast Relaxing Systems. *J. Mag. Res.* **2014**, *242*, 95–106.

(5) Walls, J. D.; Marjanska, M.; Sakellariou, D.; Castiglione, F.; Pines, A. Selective excitation in dipole coupled systems. *Chem. Phys. Lett.* **2002**, *357*, 241–248.